CARBON 92 (2015) 185–192

Available at www.sciencedirect.com

ScienceDirect

journal homepage: www.elsevier.com/locate/carbon

Efficiency enhancement from [60]fulleropyrrolidine-based polymer solar cells through N-substitution manipulation

Yulan Liang [a], Yajuan Hao [a], Xiaodong Liu [b], Lai Feng [a,*], Muzi Chen [b], Qiangqiang Tang [b], Ning Chen [b], Mingliu Tang [a], Bingbing Sun [a], Yi Zhou [b,*], Bo Song [b]

[a] College of Physics, Optoelectronics and Energy & Collaborative Innovation Center of Suzhou Nano Science and Technology, Soochow University, Suzhou 215006, China

[b] Laboratory of Advanced Optoelectronic Materials, College of Chemistry, Chemical Engineering and Materials Science, Soochow University, Suzhou 215163, China

ARTICLE INFO

Article history:
Received 4 February 2015
Accepted 4 April 2015
Available online 8 April 2015

ABSTRACT

A series of fulleropyrrolidine derivatives (FPx, x = 1–8) with alternating N-phenyl or N-methyl group were prepared as acceptors for polymer solar cells (PSCs) with the purpose of investigating the effect of N-substitutions on the photovoltaic properties of fullerene materials. More importantly, the morphology studies by means of atomic force microscopy (AFM), transmission electron microscopy (TEM), X-ray diffraction (XRD) and space charge limited current (SCLC) measurements revealed that FP1 with N-phenyl group possessed not only appropriate miscibility with P3HT but also high electron mobility, which may account for its optimal photovoltaic properties.

1. Introduction

In the past decades, polymer solar cells (PSCs) have been of great interest for the development of renewable energy technologies because of the advantages of low cost, light weight and flexibility [1–4]. Very recently, tandem PSCs have afforded power-conversion efficiencies (PCEs) exceeding 10%, showing a promising potential for commercial applications [5,6]. Specifically, intensive efforts have been devoted to improving the properties of constituent materials and morphologies of the photoactive layers, typically the blends of p-type polymers and n-type small molecules [7,8]. On the one hand, a wide range of low-bandgap polymers have been well developed [9–12]. On the other hand, fullerenes have been considered as the most widely used and highest performing n-type materials for PSCs mainly due to their high electron affinities and low reorganization energies for electron transfer [13–15]. Over the past few years, a large number of methanofullerene derivatives have been reported [16–18]. Among them, [6,6]-phenyl-C_{61}-butyric acid methyl ester ($PC_{61}BM$) as well as its C_{70} analogue (*i.e.*, $PC_{71}BM$) was demonstrated as one of the best acceptors with the widely used polymer donors such as P3HT and PTB7. To date, the state-of-the-art PSC was based on $PC_{71}BM$, giving rise to a record PCE of 11.3% [6].

Besides, other noteworthy fullerene acceptors include dihydronaphthyl-based fullerenes (NFs) [19–21] and fulleropyrrolidines (FPs) [22–26]. Some of them were found to be better acceptors than PCBM and led to higher device performances, indicating their potential as alternative acceptors to PCBM. It has been demonstrated that previously reported NF acceptors

* *Corresponding authors.*
E-mail addresses: fenglai@suda.edu.cn (L. Feng), yizhou@suda.edu.cn (Y. Zhou).
http://dx.doi.org/10.1016/j.carbon.2015.04.011
0008-6223/

feature higher LUMO levels relative to that of PCBM, resulting in enhanced photovoltaic performance through increasing the open-circuit voltage (V_{oc}) of PSC. Nevertheless, note that a series of fullerene analogues actually exhibited very different photovoltaic properties despite of their identical addition patterns as well as comparable LUMO levels [17,22,27]. It has been recognized that varying the substituents of fullerene acceptor may greatly change its electron mobility and miscibility with polymer donor. Thus, the photovoltaic properties of fullerene acceptors can be optimized by appropriately tuning their substituents.

As literature reported, the presence of aromatic substituent on the 2-position of the pyrrolidine ring is essential for the acceptor functionality of FPs. A variety of aromatic substituents, including benzene [22], thiophene [23,24], terthiophene [25] and phenothiazine [26], have been introduced to achieve optimal photovoltaic properties. However, the effect of the N-substituents in FPs has been less studied, despite the literature demonstrating their importance [22,28].

To further explore the FP family and to clarify the effect of the N-substituent on the photovoltaic properties, a series of FPs with alternating N-phenyl or N-methyl group have been synthesized and employed as acceptors for the P3HT-based PSCs. Detailed investigations regarding their optical, thermal, electrochemical and photovoltaic properties were performed. Additional experimental evidences show that the N-phenyl group has a pronounced effect on the morphology of active layer as well as the electron mobility of FP, which are all correlated to the device performance.

2. Experimental

2.1. Materials and characterization

All of the reagents were obtained from commercial suppliers and used as received unless otherwise stated. Toluene was dried over Na/benzophenoneketyl and freshly distilled prior to use. A series of benzaldehyde derivatives including 2-(hexyloxy)benzaldehyde, 2-(2-ethylhexyloxy)benzaldehyde, 2,3-bis(hexyloxy)benzaldehyde, were synthesized according to the previously published procedures [29]. High-performance liquid chromatography (HPLC) purification and analysis were performed on LC9225-370NEXT (Jai Co., Ltd.) with a Cosmosil 5PBB column (ø10 mm × 250 mm, Nacalai USA), using toluene as eluent. The ^{1}H NMR spectra were recorded on a Bruker DPX 400 (^{1}H NMR 400 MHz) spectrometer. The mass spectra were obtained using a Bruker ultrafleXtreme MALDI-TOF instrument in negative mode. UV–Vis absorption spectra were obtained using a Shimazu UV2600 UV–Vis spectrometer. Element analysis was performed on ELEMENTAR vario MICRO cube analyzer. The electrochemical cyclic voltammograms were obtained using a CHI 660E electrochemical workstation. A conventional three-electrode cell consisting of a platinum working electrode, a platinum counter-electrode, and Ag/Ag$^+$ reference electrode was used for all measurements. A solution of *o*-dichlorobenzene (*o*-DCB) containing 0.05 M (n-Bu)$_4$NFP$_6$ was used as electrolyte and the scan rate was set at 100 mV s^{-1}. All potentials were corrected against Fc/Fc$^+$. Thermogravimetric analysis (TGA) was recorded on EXSTAR TG/DTA7300 under nitrogen atmosphere at a heating rate of 10 °C min^{-1}. The differential scanning calorimetry (DSC) analysis was performed under a nitrogen atmosphere on a Mettler Instrument DSC-1 at heating rate of 10 °C min^{-1}. Morphology images of the active layers were obtained using MFP-3D-BIO (Asylum Research) atomic force microscopy (AFM) in tapping mode. Transmission electron microscopy (TEM) was conducted on a FEI TecnaiG220 instrument at 200 kV accelerating voltage. The samples for the TEM measurements were prepared as previously reported by Li et al. [30] The X-ray diffraction (XRD) patterns of the P3HT film and selected blend films (about 200 nm) on the glass substrate were recorded on a Rigaku D/Max 2000 powder diffractometer with Cu Kα radiation (40 kV, 20 mA).

Synthesis of FP1. To a toluene solution (50 mL) of C_{60} (0.14 mmol, 1 equiv.) was added 2-methoxybenzaldehyde (0.28 mmol, 2 equiv.) and N-phenyl glycine (0.56 mmol, 4 equiv.). The mixture was heated at 115 °C under an argon atmosphere for 6 h. After cooling, the reaction mixture was concentrated under reduced pressure. The crude product was first separated by silica gel column chromatography, and further purified by preparative HPLC equipped with a 5PBB column, using toluene as eluent. The purified sample was obtained as brown powder. Yield: 59% (based on consumed C_{60}). ^{1}H NMR (400 MHz, $CDCl_3$): δ (ppm) 7.76 (d, 1H), 7.39 (t, 2H), 7.28–7.21 (m, 3H), 7.02 (t, 1H), 6.93 (m, 2H), 6.83 (s, 1H), 5.69 (d, 1H), 5.19 (d, 1H), 3.78 (s, 3H). MALDI-TOF MS: $C_{75}H_{15}NO$ [M]$^-$ calc. 945.12 *m*/z; found 945.12 *m*/z. Element analysis: calcd. for $C_{75}H_{15}NO$: C 95.24, H 1.59, N 1.48%; found: C 94.92, H 1.53, N 1.51%.

Synthesis of other FPs (see Supporting information).

2.2. Device fabrication and measurements

The PSCs were fabricated with a configuration of the traditional sandwich structure (i.e., ITO/PEDOT:PSS/P3HT:FP blend/Ca/Al). The ITO glass was cleaned by a sequential ultrasonic treatment in detergent, deionized water, acetone and isopropanol. Then, a thin layer (30 nm) of PEDOT:PSS (poly(3,4-ethylenedioxythiophene):poly(styrene sulfonate)) (Baytron PVP Al 4083 Germany) was spin-coated on the ITO glass and baked at 150 °C for 30 min in air. Then, a photoactive layer (~200 nm) was prepared by spin-coating the blend solution of the P3HT donor (D) and FP acceptor (A) on the top of the PEDOT:PSS layer and annealed at 150 °C for 10 min under N_2 atmosphere. The concentration of the solution was 40 mg mL^{-1} in *o*-DCB. Finally, the Ca (20 nm)/Al (70 nm) electrode was vacuum evaporated on the photoactive layer under a shadow mask under a vacuum of ca. 10^{-5} Pa. The active area of the device was 4 mm^2. The current density–voltage (*J*–*V*) measurement of the device was performed with a Keithley 2400 SourceMeter. A xenon lamp coupled with AM 1.5 G solar spectrum filters was used as the light source, and the optical power at the sample was 100 mW cm^{-2}.

The space charge limited current (SCLC) devices or electron-only devices were fabricated with a configuration of Cs_2CO_3/active layer/Ca/Al. The Cs_2CO_3 layer (~10 nm) was firstly spin-coated on an ITO glass substrate. Then, an active layer (~200 nm) was prepared by spin-coating the *o*-DCB solution of P3HT:FP (w/w, 1:0.8) blend onto the Cs_2CO_3 layer. The films were annealed at 150 °C for 10 min. Ca (~20 nm) and

Al (~70 nm) were thermally evaporated under a shadow mask. *J–V* curves were measured using Keithley 2400 SourceMeter in dark.

2.3. Computational method

All calculations were carried out with the Gaussian 03 program package using the density functional theory (DFT) with the classical B3LYP functional, 3-21G basis set for the C, N, H, O atoms.

3. Results and discussion

3.1. Synthesis and characterizations

The FP series were synthesized via a 1,3-dipolar cycloaddition of C_{60} with N-phenyl or N-methyl substituted glycine and benzaldehyde derivatives (see Fig. 1). All the as-prepared FPs showed good solubilities in toluene, chlorobenzene and o-DCB. As expected, the FPs bearing N-phenyl group exhibited higher solubilities than the analogue bearing N-methyl group. For instance, the FP1 analogue with N-methyl group showed very poor solubility and was not suitable for PSC fabrication. The structures of FP series (*i.e.*, FP*x*, *x* = 1–8) were characterized by ^{1}H NMR and mass spectrometry.

The UV–Vis absorption spectra of the FP derivatives in toluene are shown in Fig. 2. All the FPs exhibited two characteristic peaks at 432 and 704 nm, suggesting their [6,6]-addition pattern [31]. These results indicate that the substituents attached to the pyrrolidine ring of FP derivative have little effect on the absorption spectra.

TGA was performed to evaluate the thermal stabilities of the FPs. As shown in Fig. 3 and S17–23, for all the FPs, their decomposition temperatures (T_d) at 5% weight loss are all beyond approximately 340 °C, suggesting that these FPs are stable enough for application in photovoltaic devices. It appears that replacing N-methyl group by N-phenyl group gives rise to negligible influence on the thermal properties. In addition, DSC measurement for FP1 revealed that neither endothermic nor exothermic process was observed in the range of 0–250 °C, indicating the amorphous nature of FP-type derivative (see the inset of Fig. 3).

The electrochemical properties of the FPs were investigated by means of cyclic voltammetry (CV) and all obtained potential values were summarized in Table 1 together with the estimated LUMO energy levels relative to the vaccum level. As shown in Fig. 4, all CV profiles exhibit two quasi-reversible reduction waves in the negative potential range from 0 to −2.0 V *vs* $Fc^{0/+}$, suggesting excellent electrochemical stabilities of these FPs. It can be seen that the redox waves of most FPs are slightly negatively shifted as compared to PCBM. Therefore, the LUMO levels of FPs, which can be determined from their first reduction potentials ($^{red1}E_{1/2}$ *vs* $Fc^{0/+}$) [32], are generally higher than that of PCBM (see Table 1).

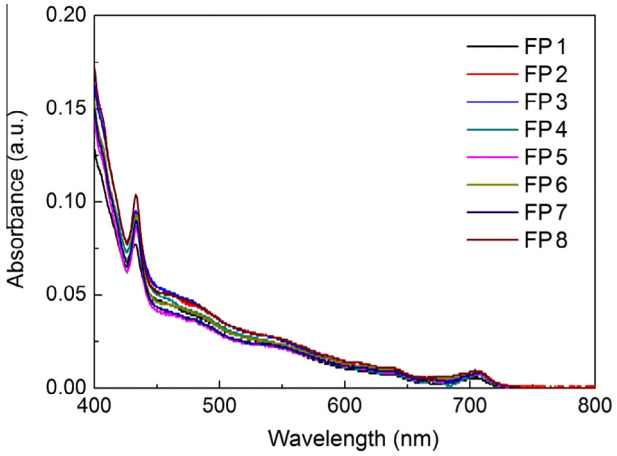

Fig. 2 – UV–Vis absorption spectra of FP*x* (*x* = 1–8) in toluene solution (2×10^{-5} M). (A color version of this figure can be viewed online.)

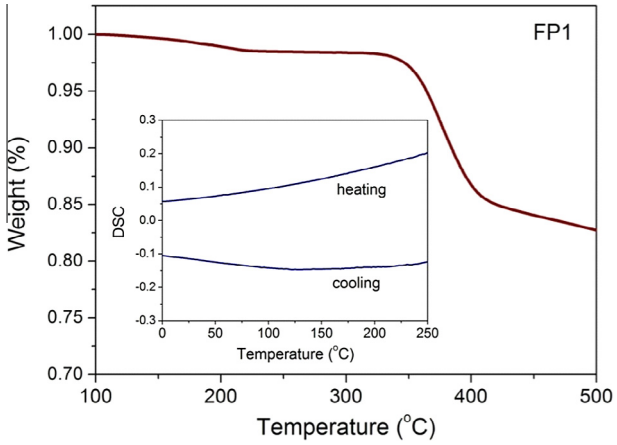

Fig. 3 – TGA plot of FP1 with a heating rate of 10 °C min^{-1} under an inert atmosphere; the inset shows the DSC plot of FP1. (A color version of this figure can be viewed online.)

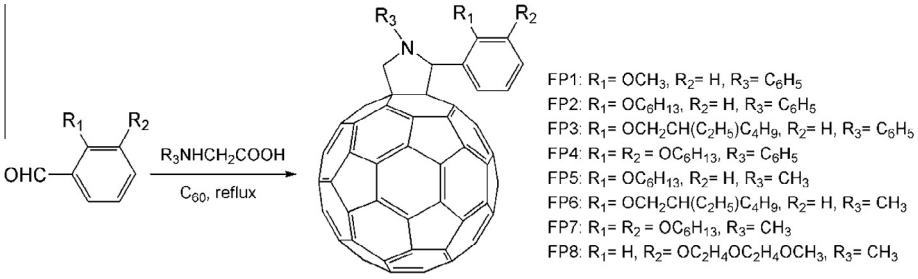

Fig. 1 – Synthetic route to FP*x* (*x* = 1–8).

Table 1 – Reduction potentials[a] and LUMO levels for FPs and PCBM.

Samples	$^{red1}E_{1/2}$	$^{red2}E_{1/2}$	LUMO[b]
PCBM	−1.19	−1.57	−3.61
FP1	−1.22	−1.60	−3.58
FP2	−1.25	−1.65	−3.55
FP3	−1.23	−1.63	−3.57
FP4	−1.19	−1.56	−3.61
FP5	−1.26	−1.67	−3.54
FP6	−1.27	−1.68	−3.53
FP7	−1.27	−1.67	−3.53
FP8	−1.22	−1.59	−3.58

[a] Potentials in V *vs* a ferrocene/ferrocenium (Fc/Fc^+) couple were measured by cyclic voltammetry in *o*-DCB solution containing 0.05 M *n*-Bu_4NPF_6 as a supporting electrolyte with a scan rate of 100 mV s^{-1}. Platinum wire, platinum wire, and Ag/Ag^+ electrode were used as the working, counter, and reference electrodes, respectively.

[b] Estimated using the following equation [32]: LUMO level = $-(4.8 + {}^{red1}E_{1/2})$ eV.

To confirm this electrochemical assertion, DFT-calculations were carried out at the B3LYP/3-21G level. The calculation results demonstrate that the geometry optimized structures have LUMO energy level of −3.36 eV for FP1, −3.35 eV for FP1 analogue and −3.41 eV for PCBM (see Fig. S24), consistent with the electrochemical results. According to the well-established principle that the V_{oc} of PSC device mainly depends on the $HOMO_D$–$LUMO_A$ gap [33,34], we predict that the FP device shows slightly higher V_{oc} than PCBM device.

3.2. *Organic photovoltaic performances*

To compare the photovoltaic properties of these variously modified FP derivatives, PSCs based on the ITO/PEDOT:PSS/P3HT:FP/Ca/Al configuration were fabricated and characterized under simulated AM 1.5 G illumination (100 mW cm^{-2}). The P3HT:FP weight ratio was optimized to 1:0.8, while a ratio of 1:1 was applied to the standard P3HT:PCBM system. The annealing process for all devices was performed at 150 °C for 10 min. The *J*–*V* curves of the devices separately using FPs and PCBM as the acceptor are shown in Fig. 5. The resulting V_{oc}, short-circuit current (J_{sc}), fill factor (*FF*), and PCE of the devices are summarized in Table 2.

As compared with the standard $PC_{61}BM$ device, FP1-based device showed slightly higher V_{oc} along with lower J_{sc} and similar *FF*. All these parameters result in a device PCE of 3.19%, which is very comparable to that of PCBM device (*i.e.*, 3.32%), suggesting good acceptor functionality for FP1. As for other N-phenyl substituted FPs, almost comparable V_{oc} and J_{sc} were obtained. However, the *FF* was remarkably decreased from 0.61 for FP1 to 0.55–0.50 for FP2–4, probably because of the long alkoxy chains in the latter, which may disrupt the optimal phase separation between donor and acceptor [22]. As the result, the PCEs of FP2–4 devices were obtained in a range of 2.83–2.38%, lower than that of FP1 device. On the other hand, the devices based on the N-methyl substituted FPs (*i.e.*, FP5–8) exhibited very poor photovoltaic performances with PCEs all below 1% (*i.e.*, ranging from

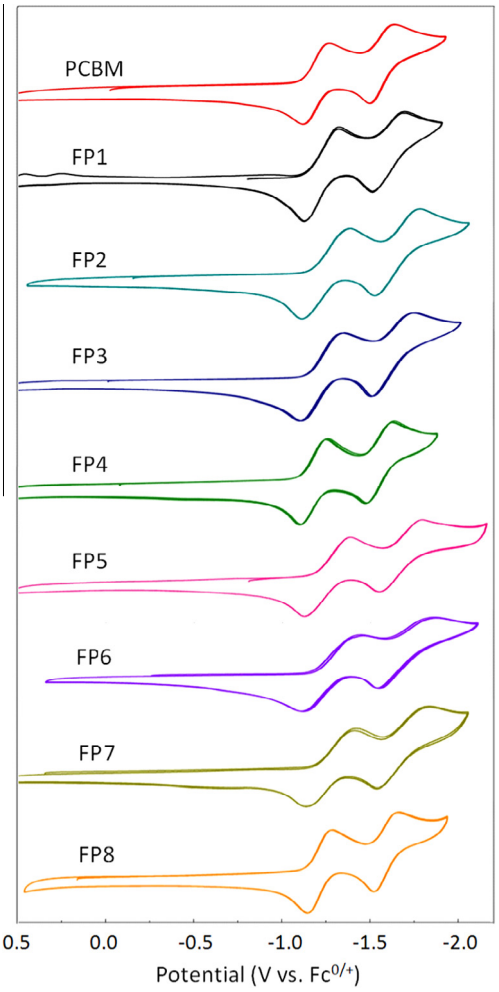

Fig. 4 – Cyclic voltammograms of FP*x* (*x* = 1–8) and PCBM in *o*-dichlorobenzene containing 0.05 M *n*-Bu_4PF_6 at 100 mV s^{-1}. (A color version of this figure can be viewed online.)

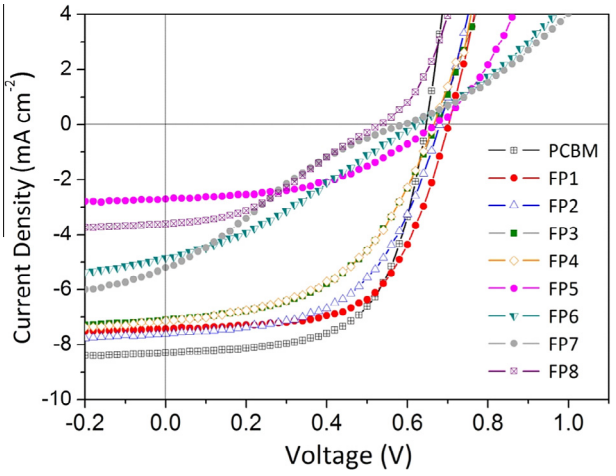

Fig. 5 – *J*–*V* curves of the PSCs based on P3HT:FP*x* (*x* = 1–8) and P3HT:PCBM blends. (A color version of this figure can be viewed online.)

Table 2 – Photovoltaic characteristics of the P3HT-based devices.

	V_{oc} (V)	J_{sc} (mA cm^{-2})	FF	PCE (%)	RMS roughness (nm)
PCBM	0.65	8.30	0.62	3.32	6.5
FP1	0.70	7.44	0.61	3.19	8.8
FP2	0.68	7.62	0.55	2.83	5.9
FP3	0.67	7.11	0.50	2.38	8.7
FP4	0.67	7.14	0.50	2.38	10.7
FP5	0.67	2.71	0.47	0.84	11.5
FP6	0.62	4.85	0.31	0.95	11.4
FP7	0.59	5.21	0.23	0.70	1.0
FP8	0.53	3.62	0.36	0.70	8.6

0.70% to 0.95%). Noteworthy is that the V_{oc} of FP5–8 are almost comparable to or slightly lower than those of FP1–4 devices, generally consistent with their LUMO levels. However, the obtained J_{sc} or *FF*s or both are substantially lower, reflecting the poor acceptor functionality for FP5–8. To this end, it appears that the N-phenyl group of FPs plays a positive role in the solar cell performance, though the mechanism is still unknown. Current studies suggest that appropriately manipulating the N-substitution of FP acceptors may lead to substantially enhanced device efficiency through increasing the J_{sc} and *FF*.

3.3. *Morphologies of the active layers*

It has been well recognized that the morphology of the photoactive layer is very important for the photovoltaic performance of PSC [35–37]. The surface morphologies of the active layers composed of P3HT and FP*x* (*x* = 1–8) after annealing at 150 °C for 10 min were studied by means of AFM with tapping mode. The AFM height and phase images are shown in Figs. 6 and 7, respectively, and the values of the root-mean-square (RMS) surface roughness for a $3 \times 3\ \mu m^2$ scan area are summarized in Table 2. For the active layers prepared from N-phenyl substituted FPs (*i.e.*, FP*x*, *x* = 1–4), the AFM height images (Fig. 6a–d) show similar surfaces with RMS roughness ranging from 5.9 to 10.7 nm. For comparison, the RMS roughness of the P3HT:PCBM blend was determined to be 6.5 nm, almost equal to that of P3HT:FP2 blend. More importantly, the extent of donor–acceptor phase separation is illustrated in the AFM phase images. As shown in Fig. 7a, P3HT and FP1 were well blended and we can see the formation of homogeneous interpenetrating networks with nanoscale phase separated domains slightly smaller than those of P3HT:PCBM (see Fig. 7i). Such morphology is considered to be beneficial to the charge separation between donor and acceptor, and agrees well with the good photovoltaic performance of FP1-based device. Besides, the panels b, c and d of Fig. 7 show larger-scale phase separation relative to that of P3HT:FP1 blend, which may account for the lower PCEs obtained from FP2–4 devices. It appears that the N-phenyl substituted FPs with additional long alkoxy chains show reduced miscibility with P3HT, giving rise to less efficient phase separation in the blend films. For further comparison, the active layers composed of N-methyl substituted FPs and P3HT were studied. Specifically, severe phase separation was observed for FP6:P3HT and FP8:P3HT blends (see Fig. 7f and h), while very fine intermixing of donor and acceptor (see Fig. 6g) for FP7:P3HT system. These morphological features

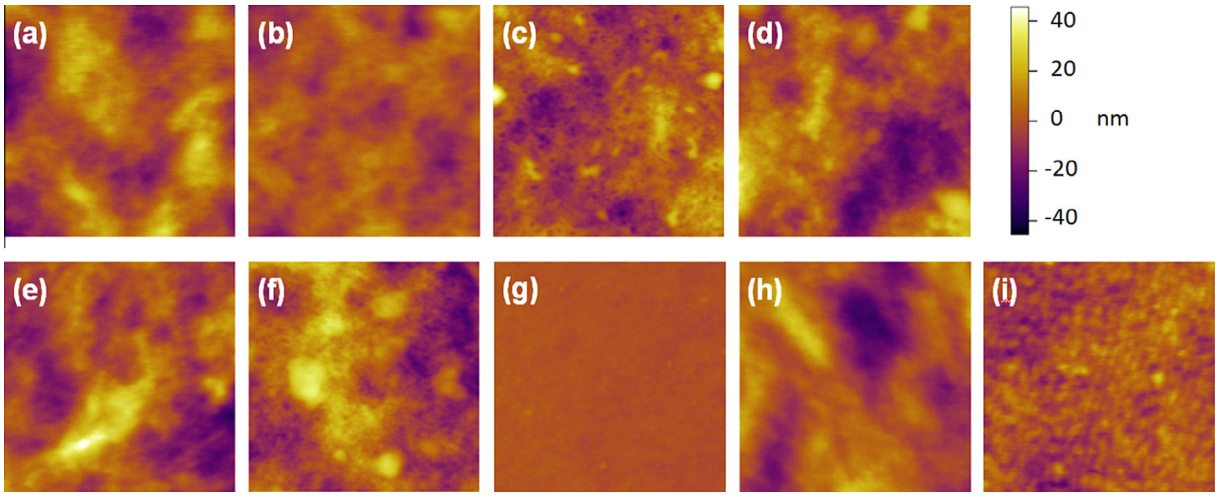

Fig. 6 – AFM height images (3 μm × 3 μm) of the active layers prepared from (a) FP1, (b) FP2, (c) FP3, (d) FP4, (e) FP5, (f) FP6, (g) FP7, (h) FP8, and (i) PCBM. P3HT was used as donor for all layers and PEDOT:PSS was used as the underlayer. All active layers were annealed at 150 °C for 10 min. (A color version of this figure can be viewed online.)

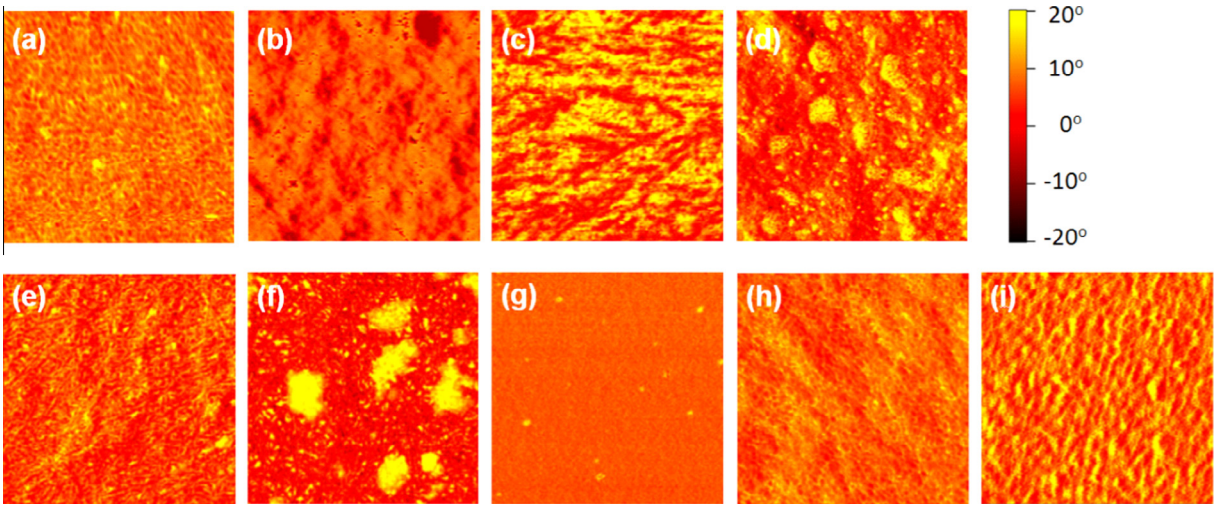

Fig. 7 – AFM phase images (3 μm × 3 μm) of the active layers prepared from (a) FP1, (b) FP2, (c) FP3, (d) FP4, (e) FP5, (f) FP6, (g) FP7, (h) FP8, and (i) PCBM. P3HT was used as donor for all layers and PEDOT:PSS was used as the underlayer. All active layers were annealed at 150 °C for 10 min. (A color version of this figure can be viewed online.)

usually lead to less efficient charge separation or recombination loss, resulting in low *FF* and J_{sc}. Nevertheless, it is noteworthy that favorable donor–acceptor separation was observed for P3HT:FP5 blend (see Fig. 7e), despite the low J_{sc} and *FF* of the devices.

TEM was used to further probe the inner-phase-separated morphology of the active layer. Fig. 8 shows the TEM images of the P3HT:FP1 and P3HT:FP5 layers with the thickness of around 100 nm. It can be seen that both the FP1 and FP5-based layers show nanoscaled and uniform phase separations, which are consistent with the morphologies observed from AFM. Moreover, to better understand the morphologies of the FP1 and FP5-based blend films, their X-ray diffraction (XRD) patterns were measured and compared with those of other blend films. As shown in Figs. S25 and S26, a diffraction peak at $2\theta = 5.3–5.7°$ corresponding to the (100) orientation of the P3HT crystallite [38] was observed in the XRD patterns of all the selected blend films. Nevertheless, as compared to those of PCBM and FP2-based blends, FP1 and FP5-based blend films show much less intensive diffraction peaks. These results confirm the thinner donor–acceptor networks in the FP1 and FP5-based blend films, which agree well with the morphologies observed in the AFM and TEM images.

3.4. *Charge mobility*

Charge mobility within an active layer is another critical factor for PSCs. Since the blend films of P3HT:FP1 and P3HT:FP5 present similar morphological features, it would be useful to evaluate their electron mobilities for better understanding their different photovoltaic properties. Herein, we adopted the SCLC method, which is suitable for determining organic semiconductors' intrinsic carrier mobility. Consistent with the former-mentioned PSCs, the SCLC devices were fabricated with a configuration of Cs_2CO_3/P3HT:FP/Ca/Al and electron mobilities were extracted using the SCLC model (see Fig. 9) [39]. As expected, FP1 possesses a good electron mobility of 1.01×10^{-3} $cm^2 V^{-1} s^{-1}$, which is much higher than that of FP5 (*i.e.*, 0.97×10^{-5} $cm^2 V^{-1} s^{-1}$). The low electron mobility of FP5 accounts for the low J_{sc} and *FF* of the device. Thus, this fact could be used to explain why FP1-based device

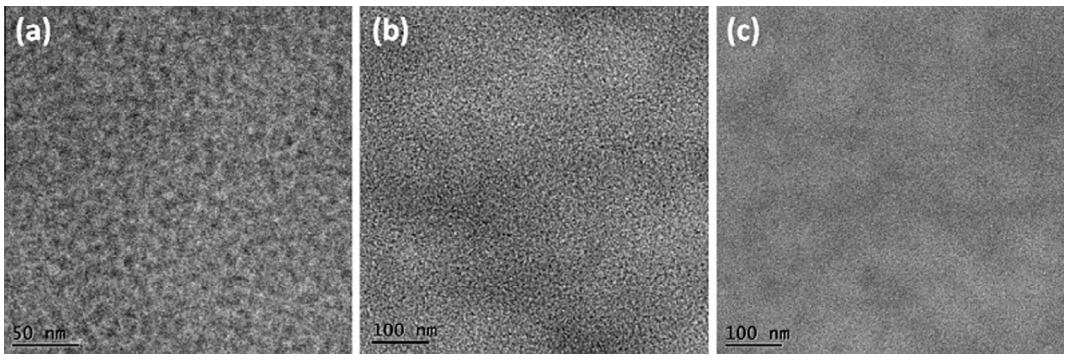

Fig. 8 – TEM images of the active layers prepared from (a), (b) P3HT:FP1 blend; (c) P3HT:FP5 blend.

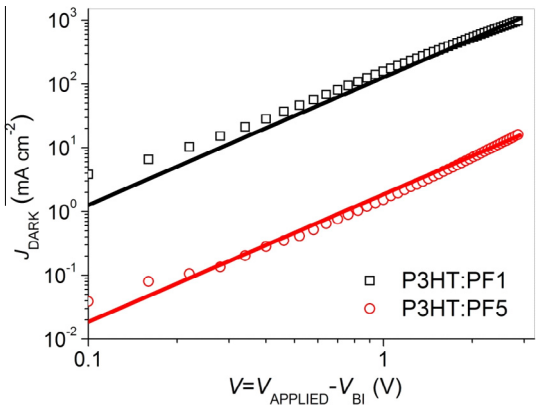

Fig. 9 – J–V characteristics of electron-only devices based on P3HT:PF1 and P3HT:PF5. (A color version of this figure can be viewed online.)

outperformed FP5 device, despite the two devices showing comparable V_{oc} as well as similar active layer morphologies.

4. Conclusions

In summary, a series of fulleropyrrolidine derivatives (FPx, x = 1–8) with alternating N-phenyl or N-methyl group have been prepared as acceptor materials for PSCs. Although all these FPs possess similar optical, thermal and electrochemical properties as well as comparable LUMO levels, PSCs using FPx as acceptor and P3HT as donor showed very different photovoltaic properties. Generally, the devices based on the N-methyl substituted FPs demonstrated very poor PCEs (all below 1%), while those based on the N-phenyl substituted FPs gave rise to much better PCEs ranging from 2.38% to 3.19%, indicating the positive role of N-phenyl group in the photovoltaic properties of FPs. Furthermore, the morphology studies by means of AFM, TEM, XRD and SCLC measurements revealed that, as compared to other FPs, FP1 showed not only favorable miscibility with P3HT but also higher electron mobility, which may account for its optimal photovoltaic performance. We also anticipate additional improvements in the photovoltaic performance by further optimizing the structure of the FP derivative.

Acknowledgments

This work is the supported in part by the NSFC (51372158, 51303118, 91333204), the NSF of Jiangsu Province (BK2012611, BK20130289). Jiangsu Specially Appointed Professor Program (SR10800113), the Project for Jiangsu Scientific and Technological Innovation Team (2013), the Ph.D. Programs Foundation of Ministry of Education of China (20133201120008), the Scientific Research Foundation for Returned Scholars, Ministry of Education of China, and a Project Funded by the Priority Academic Program Development of Jiangsu Higher Education Institutions (PAPD).

Appendix A. Supplementary data

Supplementary data associated with this article can be found, in the online version, at http://dx.doi.org/10.1016/j.carbon.2015.04.011.

REFERENCES

[1] Günes S, Neugebauer H, Sariciftci NS. Conjugated polymer-based organic solar cells. Chem Rev 2007;107(4):1324–38.
[2] Thompson BC, FréchetJ MJ. Polymer–fullerene composite solar cells. Angew Chem Int Ed 2008;47(1):58–77.
[3] Dennler G, Scharber MC, Brabec CJ. Polymer–fullerene bulk-heterojunction solar cells. Adv Mater 2009;21(13):1323–38.
[4] Delgado JL, Bouit P-A, Filippone S, Herranz MÁ, Martín N. Organic photovoltaics: a chemical approach. Chem Commun 2010;46(27):4853–65.
[5] You J, Dou L, Yoshimura K, Kato T, Ohya K, Moriarty T, et al. A polymer tandem solar cell with 10.6% power conversion efficiency. Nat Commun 2013;4:1446.
[6] Zhou H, Zhang Y, Mai C-K, Collins SD, Bazan GC, Nguyen TQ, et al. Polymer homo-tandem solar cells with best efficiency of 11.3%. Adv Mater 2015;27(10):1767–73.
[7] He Z, Zhong C, Su S, Xu M, Wu H, Cao Y. Enhanced power conversion efficiency in polymer solar cells using an inverted device structure. Nat Photonics 2012;6:591–5.
[8] Li Y. Molecular design of photovoltaic materials for polymer solar cells: toward suitable electronic energy levels and broad absorption. Acc Chem Res 2012;45(5):723–33.
[9] Chen Y-C, Hsu C-Y, Lin RY-Y, Ho K-C, Lin JT. Materials for the active layer of organic photovoltaics: ternary solar cell approach. ChemSusChem 2013;6(1):20–35.
[10] Cheng Y-J, Yang S-H, Hsu C-S. Synthesis of conjugated polymers for organic solar cell applications. Chem Rev 2009;109(11):5868–923.
[11] Chen J, Cao Y. Development of novel conjugated donor polymers for high-efficiency bulk-heterojunction photovoltaic devices. Acc Chem Res 2009;42(11):1709–18.
[12] Meager I, Ashraf RS, Mollinger S, Schroeder BC, Bronstein H, Beatrup D, et al. Photocurrent enhancement from diketopyrrolopyrrole polymer solar cells through alkyl-chain branching point manipulation. J Am Chem Soc 2013;135(31):11537–40.
[13] Kirner S, Sekita M, Guldi DM. 25th Anniversary article: 25 years of fullerene research in electron transfer chemistry. Adv Mater 2014;26(10):1482–93.
[14] Li C-Z, Yip H-L, Jen AK-Y. Functional fullerenes for organic photovoltaics. J Mater Chem 2012;22:4161–77.
[15] Liu T, Troisi A. What makes fullerenes acceptors special as electron acceptors inorganic solar cells and how to replace them. Adv Mater 2013;25(7):1038–41.
[16] Yu G, Gao J, Hummelen JC, Wudl F, Heeger AJ. Polymer photovoltaic cells: enhanced efficiencies via a network of internal donor-acceptor heterojunctions. Science 1995;270(15):1789–91.
[17] Troshin PA, Hoppe H, Renz J, Egginger M, Mayorova JY, Goryachev AE, et al. Material solubility-photovoltaic performance relationship in the design of novel fullerene derivatives for bulk heterojunction solar cells. Adv Funct Mater 2009;19(5):779–88.
[18] Zhang Y, Matsuo Y, Li C-Z, Tanaka H, Nakamura E. A scalable synthesis of methano[60]fullerene and congeners by the oxidative cyclopropanation reaction of silylmethylfullerene. J Am Chem Soc 2011;133(21):8086–9.

[19] He Y, Chen H-Y, Hou J, Li Y. Indene-C_{60} bisadduct: a new acceptor for high-performance polymer solar cells. J Am Chem Soc 2010;132(4):1377–82.
[20] He Y, Zhao G, Peng B, Li Y. High-yield synthesis and electrochemical and photovoltaic properties of indene-C_{70} bisadduct. Adv Funct Mater 2010;20(19):3383–9.
[21] He Y, Li Y. Fullerene derivative acceptors for high performance polymer solar cells. Phys Chem Chem Phys 2011;13:1970–83.
[22] Matsumoto K, Hashimoto K, Kamo M, Uetani Y, Hayase S, Kawatsura M, et al. Design of fulleropyrrolidine derivatives as an acceptor molecule in a thin layer organic solar cell. J Mater Chem 2010;20:9226–30.
[23] Kim H, Seo JH, Park EY, Kim T-D, Lee K, Lee K-S, et al. Increased open-circuit voltage in bulk-heterojunction solar cells using a C_{60} derivative. Appl Phys Lett 2010;97:193309.
[24] Yoshimura K, Matsumoto K, Uetani Y, Sakumichi S, Hayase S, Kawatsura M, et al. Thiophene-substituted fulleropyrrolidine derivatives as acceptor molecules in a thin film organic solar cell. Tetrahedron 2012;68(18):3605–10.
[25] Saravanan C, Liu C-L, Chang Y-M, Lu J-D, Hsieh Y-J, Rwei S-P, et al. [60]Fulleropyrrolidines bearing π-conjugated moiety for polymer solar cells: contribution of the chromophoric substituent on C60 to the photocurrent. ACS Appl Mater Interfaces 2012;4(11):6133–41.
[26] Mi D, Kim H-U, Kim J-H, Xu F, Jin S-H, Hwang D-H. Synthesis of a soluble fulleropyrrolidine derivative for use as an electron acceptor in bulk-heterojunction polymer solar cells. Synth Met 2012;162(5–6):483–9.
[27] Meng X, Xu Q, Zhang W, Tan Z, Li Y, Zhang Z, et al. Effects of alkoxy chain length in alkoxy-substituted dihydronaphthyl-based [60]fullerene bisadduct acceptors on their photovoltaic properties. ACS Appl Mater Interfaces 2012;4(11):5966–73.
[28] Karakawa M, Nagai T, Adachi K, Ie Y, Aso Y. N-phenyl[60]fulleropyrrolidines: alternative acceptor materials to PC61BM for high performance organic photovoltaic cells. J Mater Chem A 2014;2(48):20889–95.
[29] Boccalon M, Iengo E, Tecilla P. New meso-substituted trans-A_2B_2 di(4-pyridyl)porphyrins as building blocks for metal-mediated self-assembling of 4 + 4 Re(I)-porphyrinmetallacycles. Org Biomol Chem 2013;11(24):4056–67.
[30] Guo X, Cui C, Zhang M, Huo L, Huang Y, Hou J, et al. High efficiency polymer solar cells based on poly(3-hexylthiophene)/indene-C_{70} bisadduct with solvent additive. Energy Environ Sci 2012;5(7):7943–9.
[31] Mikroyannidis JA, Kabanakis AN, Sharma SS, Sharma GD. A simple and effective modification of PCBM for use as an electron acceptor in efficient bulk heterojunction solar cell. Adv Funct Mater 2011;21(4):746–55.
[32] Wong W-Y, Wang X-Z, He Z, Djurišić AB, Yip C-T, Cheung K-Y, et al. Metallated conjugated polymers as a new avenue towards high-efficiency polymer solar cells. Nat Mater 2007;6:521–7.
[33] Scharber MC, Mühlbacher D, Koppe M, Den KP, Waldauf C, Heeger AJ, et al. Design rules for donors in bulk-heterojunction solar cells-towards 10% energy-conversion efficiency. Adv Mater 2006;18(6):789–94.
[34] Koster LJA, Mihailetchi VD, Blom PWM. Ultimate efficiency of polymer/fullerene bulk heterojunction solar cells. Appl Phys Lett 2006;88(9):093511.
[35] Heeger AJ. 25th Anniversary article: bulk heterojunction solar cells: understanding the mechanism of operation. Adv Mater 2014;26(1):10–28.
[36] Park SH, Roy A, Beaupré S, Cho S, Coates N, Moon JS, et al. Bulk heterojunction solar cells with internal quantum efficiency approaching 100%. Nat Photonics 2009;3:297–302.
[37] Morana M, Azimi H, Dennler G, Egelhaaf H-J, Scharber M, Forberich K, et al. Nanomorphology and charge generation in bulk heterojunctions based on low-bandgap dithiophene polymers with different bridging atoms. Adv Funct Mater 2010;20(7):1180–8.
[38] Müller-Buschbaum P. The active layer morphology of organic solar cells probed with grazing incidence scattering techniques. Adv Mater 2014;26(46):7692–709.
[39] An Z, Yu J, Jones SC, Barlow S, Yoo S, Domercq B, et al. High electron mobility in room-temperature discotic liquid-crystalline perylene diimides. Adv Mater 2005;17(21):2580–3.